Chaotic trapping phenomena in extended systems

Gianni Pedrizzetti
Dipartimento di Ingegneria Civile, Università di Firenze, via Santa Marta 3, 50139 Firenze, Italy

James B. Kadtke
Institute for Pure and Applied Physical Sciences, University of California at San Diego, La Jolla, California 92093-0075

Harry H. Luithardt
Institute for Nonlinear Science, University of California at San Diego, La Jolla, California 92093-0402
(Received 2 June 1993)

The interaction of fluid structures with bodies in the flow field is an important and topical research area, and recently a new phenomena has been proposed involving the metastable capture of vortex structures by bluff bodies. The fundamental mechanism for this capture phenomenon is the generation of chaos in the perturbed Hamiltonian point-vortex model for the system, and a variety of numerical results have been quoted in this framework. In this paper, we present the results of a study of the capture phenomenon in a more realistic context, i.e., by a numerical solution of the Navier-Stokes equations for the system. A mixed spectral–finite-difference numerical scheme is used to study the interactions of extended vorticity profiles with a bluff body and comparisons are made to the previous point-vortex results. In general, we find that the capture phenomenon exists generically in the extended system and that many of the physical characteristics of the phase-space topology of the Hamiltonian system persist, even for relatively large vortex diameters. For even larger profiles, we find that the internal degrees of freedom of the vortex structure are sufficient to generate a trapping phenomena without an explicit perturbation and that several additional types of dynamical behavior occur. We comment on the general mechanisms for these phenomena and make connections with possible applications to physical systems.

PACS number(s): 05.45.+b, 47.32.Cc, 47.52.+j, 83.50.Ws

I. INTRODUCTION

The dynamics of the interaction of fluid flows with physical bodies represents a complex and important research area in fluid dynamics, with applications to turbulence theory, hydrodynamics, aerodynamics, and atmospherics among others. In three-dimensional flows, the large computational effort required to solve the Navier-Stokes equation has motivated the search for asymptotic or reduced descriptions of such flows [1–3]. The study of such interactions in corresponding two-dimensional (2D) flows has received much attention recently, encouraged by the use of numerical calculations which can within certain limits handle many problems by direct Navier-Stokes integration.

In recent years a new mechanism termed "chaotic scattering," which arises generically from the existence of chaotic behavior in unbounded systems [4,5], has also been considered for the interaction of vortex structures incident upon bluff bodies embedded in the fluid flow. A similar mechanism has recently been shown analytically to exist in simple models of the interactions of vortices with bluff bodies, and the related dynamical phenomenon consists of a chaotic interaction of the vortices with the body [5]. The physical significance of the chaotic behavior of an impinging vortex in the vicinity of the body is that it can result in metastable "capturing" of the vortex around the body, which is extremely sensitive to initial conditions and which produces very rich dynamics. Numerical simulations indicate that during a chaotic capture event, the vortex can spend unusually long periods of time interacting with the body, and resultant pressure variations on the body have been demonstrated to become nearly three orders of magnitude larger than would be expected in the absence of chaos [5]. Such a mechanism may therefore have significant implications for such physical systems as aircraft wings, water craft, piers, and cables among others.

To date, previous investigations of the chaotic trapping mechanism have all utilized an inviscid, point-vortex Lagrangian framework for the analysis and simulations. In this paper, we present simulations of the mechanism based on a semispectral implementation of the viscous Navier-Stokes equations for the idealized system presented in Ref. [6]. The principal aim of the present study is to generalize the model and observe the differences in the time evolution of an extended vortex system. In order to draw comparisons to the previous work, the influence of viscosity is made minimal by enforcing a free-slip boundary condition on the body surface and by setting the Reynolds number at 1000; dissipative phenomena still contained in the evolution of the flow, unavoidable in such a simulation, are then discussed. Further studies utilizing the full viscous dynamics for extended systems, which includes no-slip boundary conditions and the resulting boundary layer vortex shedding, are in progress [7]. These studies present additional complexities by combining the trapping behavior presented here with the in-

teraction of the principal vortex structure and the shed vorticity. Although the present work corresponds roughly to an ideal hydrodynamics, such simulations utilizing the Navier-Stokes (NS) framework are considerably more physically credible than the point-vortex approaches. They may therefore provide a critical link between simple numerical simulations and observation of the phenomena in real physical systems, and represent a second approximation to real fluid systems. Furthermore, they also provide a quantitative measure to gauge the utility of the idealized point-vortex calculations, and here we have found some striking comparisons.

The principal aim of this paper is therefore to demonstrate the existence of the chaotic trapping mechanism in an extended fluid system, and to make connection with some of the previous analyses which utilized reduced point-vortex approaches. We present and discuss examples of chaotic capture events in the NS simulation, which are very similar to those observed in the previous simulations. We also investigate more extended vorticity distributions for which the point-vortex models are not applicable, and demonstrate behavior such as partial capture of a fraction of the original vorticity distribution. Section II of this paper reviews the generic system being studied along with previous results on the chaotic capture mechanism. Section III describes the implementation of the Navier-Stokes framework, and relevant numerical issues. Section IV describes numerical results for the simulations, and Sec. V gives conclusions and future directions.

II. BACKGROUND

To review the original two-dimensional Lagrangian description of the problem, we recall the formulation for the simplest case of a point vortex in a uniform background potential flow incident on a bluff body, in this case a circular boundary. Figure 1 shows a schematic of the physical system defining the problem. The 2D point-vortex formulation yields a Hamiltonian system with one degree of freedom for the single vortex case, which is an integrable system if the background flow is time independent [5]. The problem is made dimensionless by using the cylinder radius as the unit of length, and the uniform flow velocity as the unit velocity scale. Representative fluid flow contours can be traced out using the equienergy lines of the Hamiltonian, given by

$$H=-(\sin\theta/r)(r^2-1)+(\sigma/2)\ln(r^2-1)\ , \tag{1}$$

where we use a polar coordinate system (r,θ), and all variables have been rescaled to yield a single nondimensional parameter σ (equal to dimensionless vortex circulation divided by 2π). In general, variation of σ changes the topology of the flow field [5]. The fluid flow contours for a representative value $\sigma=-2.962\,96\ldots$ are shown in Fig. 2.

The flow geometry in Fig. 2 contains a single hyperbolic fixed point (i.e., stagnation point) in the flow field with a corresponding separatrix which extends to infinity in the plus/minus x-directions. More complex systems can also be defined if one adds a constant circulation about the body (not discussed in this paper), and such generalizations have the effect of adding additional elliptic and hyperbolic fixed points. The positions of the fixed points and the geometry of the connections of their separatrices define the topology of the unperturbed flow field, in the sense of determining which regions of the flow can "communicate." Nearly a dozen distinct flow topologies have been identified for the Hamiltonian system to date.

Chaotic behavior can be generated in the above system in a simple way by the introduction of a perturbation, and in the original formulation this was chosen to be a sinusoidal oscillation of the body in the direction of the flow field. Using the Melnikov integral technique, one can show analytically that such a perturbation generates a homoclinic tangle around the hyperbolic points of the flow field, and hence generates chaotic motion of the vor-

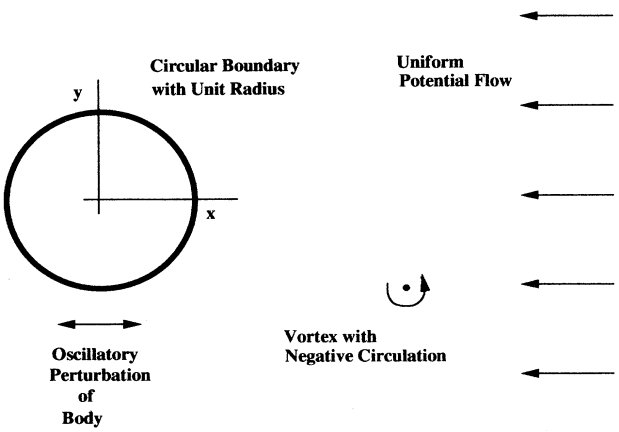

FIG. 1. Schematic of the physical system, showing lines of constant flow, the circular body, the incident vortex, and the perturbation direction.

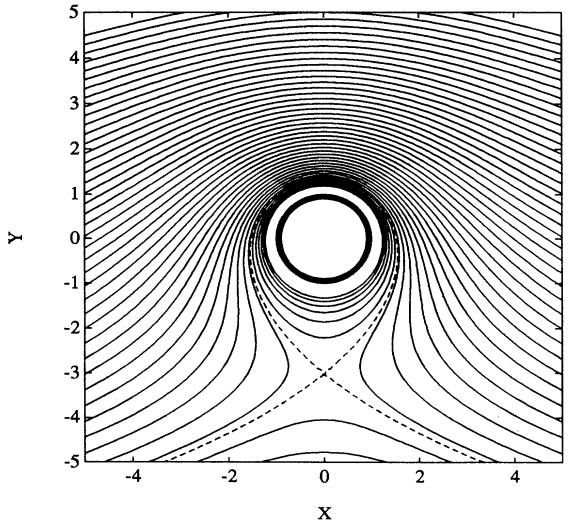

FIG. 2. Iso-Hamiltonian curves (contours of H from -10 to $+1$ by 0.25) for a point vortex of intensity $\sigma=-2.962\,96\ldots$, constant flow, in the presence of a cylindrical body.

tex which is confined to a stochastic layer around the separatrices. Dynamically, these stochastic layers allow the exchange of phase-space volume across the separatrices and hence allow otherwise separated regions of the flow to communicate [8]. In terms of the fluid vortex motion, this means that it is possible for a vortex approaching the body to be swept across a separatrix, evolve for some period of time around the body, and eventually escape. Interestingly, in the more complex topologies that arise when one has additional circulation about the body, it is also possible for the vortex to be captured around elliptic points at some distance from the body, and to evolve in chaotic trajectories without actually circling the body.

The existence of this mechanism implies that for a system for which an incident vortex would otherwise be expected to be simply swept past a body with minimal interaction time, the vortex can now be trapped metastably with potentially far longer interaction times, as well as much closer interaction distances with resultant higher pressure fluctuations. A variety of numerical results have been previously shown which indicate that the resulting vortex dynamics can be quite rich and in some cases somewhat counterintuitive. It is interesting to note that the above system may be of purely mathematical interest as an example of an extremely simple dynamical system that exhibits relevant chaotic behavior, in a way which still has a direct physical analog. A critical element of the system is the addition of the perturbation mechanism, and the original choice of a sinusoidal oscillation along the flow direction is not aphysical, as this type of motion is often induced naturally. We note that alternate forms of perturbation which may yield chaotic trapping events are also possible, for example, inclusion of internal degrees of freedom for the vortex itself. This occurs because the only conserved quantity in these systems is energy, and hence the addition of other degrees of freedom leads generically to nonintegrability of the system. Preliminary results indicate that modeling of the vortex by a simple bound pair of like-magnitude point vortices produces chaotic trapping events without the necessity of explicit perturbation of the background flow [9].

Although the Hamiltonian point-vortex framework for this system is quite useful for obtaining analytic results and as a first-order model, the connect of its dynamics with that of an extended, real physical flow may be somewhat tenuous. This is partly because it is not immediately obvious how closely the flow field of a vortex patch system strongly interacting with a body will correspond to the phase plane of an idealized point-vortex system, i.e., it is not clear what happens to the fixed points and separatrices of the idealized model in a more realistic context. A more credible approach to the investigation of the chaotic trapping phenomenon is that of the Navier-Stokes formulation of the system. Consequently, we have performed an investigation of the properties of this system by formulating a numerical scheme for the solution of the vorticity transport using the Navier-Stokes equations. This numerical framework was used to evolve the dynamics of an extended, coherent profile of vorticity for similar system parameters as the Hamiltonian system, to determine if the qualitative features of the dynamics persist. In this extended vorticity formulation, it is more difficult to draw analogy to the fixed points and separatrices of the Hamiltonian formulation, as we expect extended stagnation "regions" and a "separatrix" which is similarly extended in space. In fact, the actual phase space of this system is technically infinite dimensional whereas the phase space of the point-vortex systems is two dimensional. In addition, we expect viscosity to play an important role, with the dissipation generally decreasing the amount of time a vortex may be expected to interact with the body due to alterations of the vorticity profile. This important point will be discussed in detail later.

Another interesting aspect of the extended system is to determine the relative sizes of the vorticity distributions for which the dynamics become qualitatively different from the point-vortex results, and to investigate the differences in dynamical behavior. Although we have identified several previously unreported features of the dynamics for large vorticity profiles, we generally find that much of the qualitative behavior of the point-vortex simulations persist even for relatively large vorticity distributions.

III. NAVIER-STOKES NUMERICAL SIMULATIONS

To investigate the dynamics of the chaotic vortex-body interactions of an extended vortex structure, we conducted simulations of the system based on direct numerical solution of the two-dimensional Navier-Stokes equations using a mixed spectral–finite-difference method. For this formulation, the equations of motion are written in the vorticity-stream function (ω,ψ) form. Using cylindrical coordinates (r,θ), the velocity field is given by

$$V_r=(1/r)\frac{\partial\psi}{\partial\theta} \quad \text{and} \quad V_\theta=-\frac{\partial\psi}{\partial r}$$

for the radial and tangential velocities, respectively. The dimensionless equations can be written as

$$\frac{\partial\omega}{\partial t}=(1/r)\left[\frac{\partial\psi}{\partial r}\frac{\partial\omega}{\partial\theta}-\frac{\partial\psi}{\partial\theta}\frac{\partial\omega}{\partial r}\right]+(1/\mathrm{Re})\nabla^2\omega\ , \tag{2}$$

$$\omega=-\nabla^2\psi\ , \tag{3}$$

where the operator

$$\nabla^2=(1/r)\frac{\partial}{\partial r}\left[r\frac{\partial}{\partial r}\right]+(1/r^2)\frac{\partial^2}{\partial\theta^2}$$

and the Reynolds number $\mathrm{Re}=U_0R_0/\nu$, with ν being the kinematic viscosity.

Dynamically the most interesting behavior, i.e., requiring the greatest resolution, occurs close to the body, and hence we introduce a stretched coordinate in the radial direction. This stretching permits us to maintain the required resolution close to the body while extending the computational domain to a sufficiently large distance from the cylinder needed to approximate a physically unbounded flow. Both of these requirements are met using a reasonable number of grid cells; in our simulations, we

employed a 128 by 128 grid. A new radial coordinate η is defined such that

$$\eta=\ln[(r-1+a)/a] \ , \quad \text{or } r(\eta)=ae^{\eta}+1-a \ ,$$

where a is the stretching parameter. Using this definition, Eqs. (2) and (3) then become

$$\frac{\partial\omega}{\partial t}=(1/rae^{\eta})\left[\frac{\partial\psi}{\partial\eta}\frac{\partial\omega}{\partial\theta}-\frac{\partial\psi}{\partial\theta}\frac{\partial\omega}{\partial\eta}\right]+(1/\mathrm{Re})\nabla^2\omega \tag{4}$$

and

$$\omega=-\nabla^2\psi \ , \tag{5}$$

where

$$\nabla^2=(1/ae^{\eta})^2\frac{\partial^2}{\partial\eta^2}+[(1/rae^{\eta})-(1/ae^{\eta})^2]\frac{\partial}{\partial\eta}+(1/r^2)\frac{\partial^2}{\partial\theta^2}$$

and $r=r(\eta)$. To the dynamical equations, we must add boundary conditions at the body surface and at the exterior "cutoff" surface of the computational domain. The cylinder surface boundary conditions should approximate the free-slip boundary conditions commonly used in inviscid simulations, and the exterior boundary conditions should be chosen to approximate as closely as possible an unbounded flow. We will discuss both sets of boundary conditions in detail after describing our time-evolution scheme.

The external flow at infinity is given by $U(t)=1+\epsilon\sin(\Omega t+\phi)$, and the irrotational solution corresponding to it is $\psi_0=-U(t)(r-1/r)\sin\theta$. We subtract this known contribution to the stream function and consider the correction to it, $\hat{\psi}=\psi-\psi_0$ as the unknown (note that $\nabla^2\psi_0=0$ and $\omega_0=0$). Using this variable, Eqs. (4) and (5) are then given by

$$\frac{\partial\omega}{\partial t}=(1/rae^{\eta})\left[\frac{\partial\hat{\psi}}{\partial\eta}\frac{\partial\omega}{\partial\theta}-\frac{\partial\hat{\psi}}{\partial\theta}\frac{\partial\omega}{\partial\eta}\right]+(U/rae^{\eta})\left[-ae^{\eta}(1+1/r^2)\sin\theta\frac{\partial\omega}{\partial\eta}+(r-1/r)\cos\theta\frac{\partial\omega}{\partial\eta}\right]+(1/\mathrm{Re})\nabla^2\omega \tag{6}$$

and

$$\omega=-\nabla^2\hat{\psi} \ . \tag{7}$$

Since all the quantities are periodic in the θ direction, we introduce a spectral representation in θ expressing all quantities as Fourier series:

$$\omega(t,\eta,\theta)=\sum_n\omega_n(t,\eta)e^{in\theta} \ , \quad \hat{\psi}(t,\eta,\theta)=\sum_n\psi_n(t,\eta)e^{in\theta} \ , \tag{8}$$

where $-\infty\le n\le\infty$ and $i=\sqrt{-1}$.

By substituting representation (8) in Eqs. (6) and (7), we get the set of equations to be solved numerically:

$$\frac{\partial\omega_n}{\partial t}=(1/rae^{\eta})\left[\frac{\partial\hat{\psi}}{\partial\eta}\frac{\partial\omega}{\partial\theta}-\frac{\partial\hat{\psi}}{\partial\theta}\frac{\partial\omega}{\partial\eta}\right]_n+(U/2rae^{\eta})\left\{-ae^{\eta}(1+1/r^2)[(n-1)\omega_{n-1}-(n+1)\omega_{n+1}]+(r-1/r)\left[\frac{\partial\omega_{n-1}}{\partial\eta}+\frac{\partial\omega_{n+1}}{\partial\eta}\right]\right\}+(1/\mathrm{Re})\nabla^2\omega \tag{9}$$

with

$$\omega_n=-\nabla^2\psi_n \quad \text{and} \quad -\infty\le n\le\infty \ . \tag{10}$$

To Eqs. (9) and (10) we must add the boundary conditions of the vorticity and stream function at infinity and on the body surface. At infinity, or more correctly on the outer boundary of our computational domain, we impose the condition that the flow is irrotational, and the velocity is given by the irrotational solution

$$\frac{\partial\psi_n}{\partial r}\to 0 \quad \text{and} \quad \omega_n\to 0 \quad \text{when } \eta\to\infty \ . \tag{11}$$

On the body surface we must impose the condition that the wall is a streamline, or rather $\partial\hat{\psi}/\partial\theta=0$. Using the spectral representation we have

$$\psi_n=0 \quad \text{when } \eta=0 \ . \tag{12}$$

The Navier-Stokes equations are a second-order system of partial differential equations and require a second boundary condition on the body surface. In general, this is usually chosen as the "no-slip" condition, but here we seek to apply an inviscid condition. Physically, we regard the boundary layer thickness as smaller than the

grid spacing. This condition may be heuristically simulated by using a slip condition and evaluating the stream function from (12) and the vorticity from a Neumann condition

$$\frac{\partial \omega_n}{\partial r}=0 \quad \text{at } \eta=0 \; . \tag{13}$$

This condition is typically imposed in inviscid flow simulations. The validity of this approach is as yet theoretically unproven for viscous flows, however, it has been widely used in the literature and shown to give meaningful results [10,11].

In the numerical implementation, a finite number of spectral modes is chosen and the radial direction η is discretized by considering a finite number of grid points between the body surface and a large but finite distance corresponding to a maximum radius. Equations (9) and (10), and the conditions (11) and (13) are discretized in the radial direction η by second-order finite differencing. The nonlinear terms in Eq. (9) are calculated by direct convolution in Fourier space (full spectral). Time evolution is accomplished by using a second-order Adams-Bashforth scheme. In the results presented below, when not otherwise specified, we used a maximum radius equal to 80 (see Ref. [12] and references therein for a discussion of how to choose a "cutoff" distance for this exterior domain radius). Also, we used 128 grid points, a stretching parameter $a=0.05$, 64 modes in the tangential direction, and a time step of 0.0005. We have empirically found these parameters to be optimal with respect to computational efficiency and numerical stability of our solutions.

IV. NUMERICAL RESULTS

Our general approach to searching for extended capture events was to replace the idealized point-vortex positions of the original systems with a vortex patch which was of appreciable extent on the scale of the physical system, and yet still small enough so that we may expect the main qualitative features of the previous work to persist. Problems of numerically resolving sharp vorticity gradients suggest that we define the vortex patch by imposing a smooth vorticity profile. A Gaussian distribution, which asymptotically can be made to yield the point-vortex Dirac distribution, is an obvious choice. Therefore, the initial vorticity distribution is assumed to have a two-dimensional, radially symmetric Gaussian shape, centered on (x_0,y_0) and of typical half-width of one standard deviation S, i.e.,

$$\omega=(\sigma/S^2)\exp\{-[(x-x_0)^2+(y-y_0)^2]/2S^2\} \; . \tag{14}$$

Now consider a concentrated vortex, i.e., S small with respect to cylinder radius. When the uniform flow is unperturbed ($\epsilon=0$) the evolution of the vortex patch is very similar to what is obtained with the point-vortex model. Generally, in this uniform-flow regime, only small differences are observed compared to the original point-vortex model, and these are due to the finite size of the vortex distribution, as well as in part to the finiteness of the integration domain (in the point-vortex model the boundary condition is analytically imposed at infinity). In Fig. 3 we show two trajectories of the extended vortex patch whose σ parameter is equal to that used in the point-vortex case reported in Fig. 2 of Ref. [6], i.e., $\sigma=-2.962\,96\ldots$. The parameters for the extended vortex simulations are $S=0.25$ and an initial condition of $x_0=2.0, y_0=-4.0$, and $x_0=2.0, y_0=-4.2$, respectively. Each contour snap shot corresponds to 0.5 time units, and each contour level corresponds to a relative vorticity level chosen to be 55% of maximum vorticity at the same instant. These trajectories are computed by full Navier-Stokes integration as described in the previous section, with a corresponding Reynolds number Re equal to 1000. If compared with the original point-vortex trajectories presented in Fig. 2 of Ref. [6], they correspond to trajectories above and below the original separatrix, even though in the extended case these trajectories correspond in actuality to a projection into two dimensions of the extended system's high-dimensional phase space, and such a separatrix is no longer a well-defined object. The influence of dissipation, in the absence of vortex shedding, is limited to a slow spreading of the vorticity distribution, as can be observed from the plot. Dissipation makes the system irreversible, and destroys the symmetry with respect to the $x=0$ plane which was present in the ideal point-vortex calculation. We emphasize that although the value $S=0.25$ already yields a patch of significant size measured on the scale of the body, we still observe the persistence of the phase-space structure of the point-vortex system.

In Ref. [6] it was shown that an oscillation of the external flow (i.e., of the body) can induce a chaotic capture of the vortex, which must also result in detrapping in some

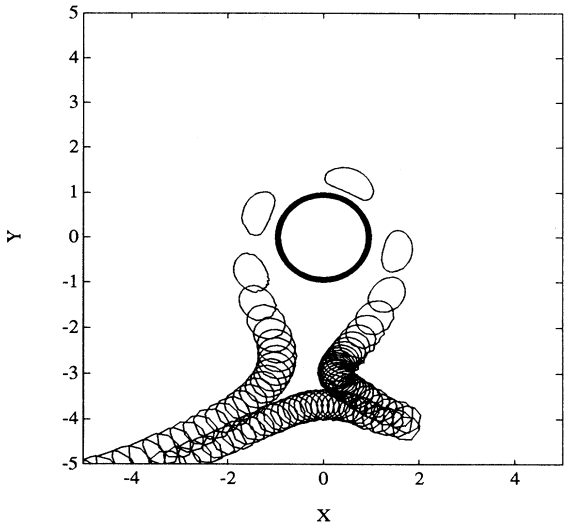

FIG. 3. Evolutions of two separate Gaussian extended vortices of intensity $\sigma=-2.962\,96\ldots$, and size $S=0.25$ in a constant flow, in presence of a cylindrical body. Initial position of vortex centers are $x_0=2, y_0=-4$ (above the body) and $x_0=2, y_0=-4.2$. A vorticity contour (at 55% of instantaneous maximum vorticity value) is drawn every 0.5 time units.

finite time interval. Physically, oscillation implies a stochastization of the trajectories around the hyperbolic point and hence the vortex can, for particular initial conditions and oscillation frequencies, cross a separatrix and evolve around the body. In the extended dissipative system presented here the number of revolutions that we expect to be possible for the vortex is reduced because the viscous diffusion of vorticity implies a continuing increase in the distance of the vortex from the body, due to a shifting of the homoclinic loop toward the cylinder. Additionally, the finiteness of the extended vortex prevents it from passing very close to the body without strong distortion, as was observed in the point-vortex model, and hence identical trajectories cannot be followed for particular events. Although these dynamical mechanisms are fundamentally different than the inviscid dynamics of the original model, we nevertheless intuitively expect that capture phenomena still exist, based on the observed robustness of the phase-space topology of the original system in the extended framework.

In Figs. 4 and 5, we present two capture events for the extended system. In both cases the vortex system has the same parameter σ as in the previous calculations, the same $\mathrm{Re}=1000$ and the same width $S=0.25$, and computations start with the vortex at $x_0=2.0, y_0=-4.0$. The figures plot vortex trajectories at several instants 0.5 time units apart by plotting at each instant a contour of the vorticity level (equal 55% of maximum vorticity at the same instant). The perturbed external flow is given by $U(t)=1+\epsilon\sin(\Omega t+\phi)$. In the evolution presented in Fig. 4, the perturbation amplitude is $\epsilon=0.2$, with frequency $\Omega=0.5$ and phase $\phi=1.3$. The vortex is shown arriving from "upstream" of the body, where it then is captured and makes nearly two complete loops around the body before escaping. For the evolution presented in Fig. 5, the corresponding system parameters are $\epsilon=0.2, \Omega=1.0, \phi=1.8$. In this case, the vortex arrives from upstream and then slows critically for some time in the region where the hyperbolic point of the point-vortex system was located. The vortex then leaves the vicinity of the hyperbolic point and is captured for nearly three complete revolutions around the body before escaping. Due to the computational intensiveness of the numerical scheme, the parameters for the capture events could not be found by trial and error as for the point-vortex case, but were determined by searching in the neighborhood of parameters which yielded large chaotic regions in the point-vortex models. The existence of these capture events show the extreme sensitivity to initial conditions, as well as the system parameters ϕ and the perturbation frequency Ω, that is to be expected of a chaotic dynamical phenomena. It is observed that small changes in one of these parameters can make the vortex pass above or below the body without being captured, or can dramatically change the capture dynamics, and hence the generic global dynamical characteristics of the point-vortex model are preserved.

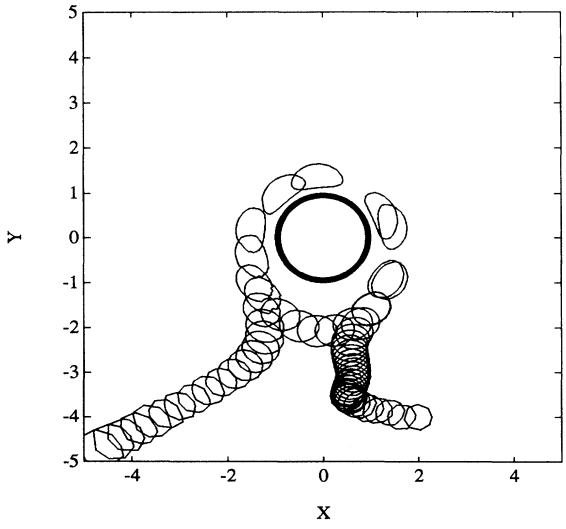

FIG. 4. Evolution of a Gaussian extended vortex of intensity $\sigma=-2.962962\ldots$, and size $S=0.25$ in a perturbed stream flow, in presence of a cylindrical body. Initial position of vortex center is $x_0=2, y_0=-4$. A vorticity contour (at 55% of instantaneous maximum vorticity value) is drawn every 0.5 time units. Perturbation is given by $U(t)=0.2\sin(0.5t+1.3)$.

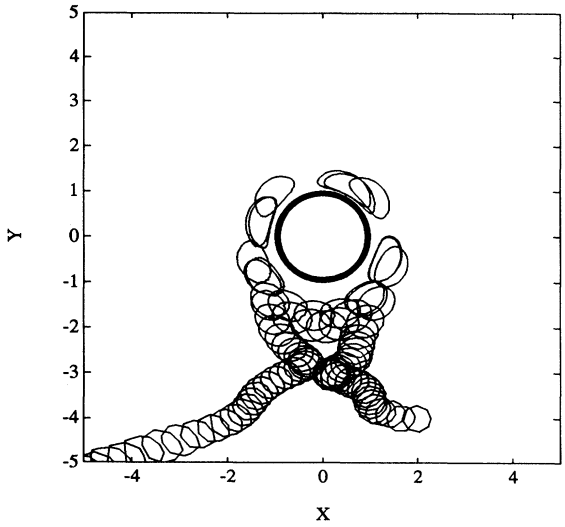

FIG. 5. Evolution of a Gaussian extended vortex of intensity $\sigma=-2.962962\ldots$, and size $S=0.25$ in a perturbed stream flow, in the presence of a cylindrical body. Initial position of vortex center is $x_0=2, y_0=-4$. A vorticity contour (at 55% of instantaneous maximum vorticity value) every 0.5 time units. Perturbation is given by $U(t)=0.2\sin(1.0t+1.8)$.

These results indicate that the point-vortex model at least qualitatively captures much of the fundamental dynamical behavior of the extended system, when the extended vorticity distribution is relatively concentrated. For more extended vorticity distributions, we expect to see increasing discrepancies with the point-vortex model results. In the point vortex case a length scale induced by the perturbation amplitude exists, which is related to stochastization of the homoclinic loop, i.e., related to the

separatrix oscillation amplitude. In the extended simulations, the finite S and the resultant "internal" dynamics of the vortex patch imposes a new length scale not present in the point-vortex model, which can in theory induce stochastization of the system by itself, even in the absence of flow oscillation. More specifically, in analogy to the point-vortex model this length scale can be associated with a perturbation to the integrable dynamics of the center of vorticity of a cluster of n-point vortices. In this model the patch is replaced by this set of bound vortices whose relative dynamics represents the internal degrees of freedom of the patch [7]. We expect that the internal degrees of freedom in the extended system itself may induce sufficient perturbation to the center of vorticity dynamics to create chaotic trapping of the vortex. Additionally, we have observed that in the absence of external perturbation, a significantly extended vortex straddling the "separatrix" can divide into two parts because of the divergence of the streamlines approaching the original hyperbolic point. This phenomenon should in principle be present for any nonzero value of S, however, we have presently only observed it occurring for values of S greater than about 0.5, whereas for smaller S it has been observed that the vortex prefers to stagnate in the "hyperbolic region" before moving either above or below the cylinder. We note, however, that the rather large computational requirements of our simulations have restricted the size of the parameter space that we have been able to explore so far. To date, it is not yet clear at which internal length-scale threshold that bifurcation from point particlelike dynamics to full spatiotemporal complexity occurs, although further investigations are in progress with models of intermediate complexity.

To illustrate the dynamics representative of a large spatially extended system, we present in Fig. 6 the evolution of a vortex distribution with the same σ and Re as before, however, now with $S=0.75$ and initial condition $x_0=3.0, y_0=-4.0$. The system consists of a uniform flow with no explicit perturbation. A completely different dynamics can be observed, where the internal dynamics of the spatial vorticity distribution plays a major role. Here, we see an interaction where the vortex is captured around the body initially, but where part of the vortex then escapes and part remains captured (at least for the time period of the simulation). In this case, too, we observe a sensitivity to initial condition of the system, with small changes in parameters resulting in the vortex passing either above or below the body, modifying the

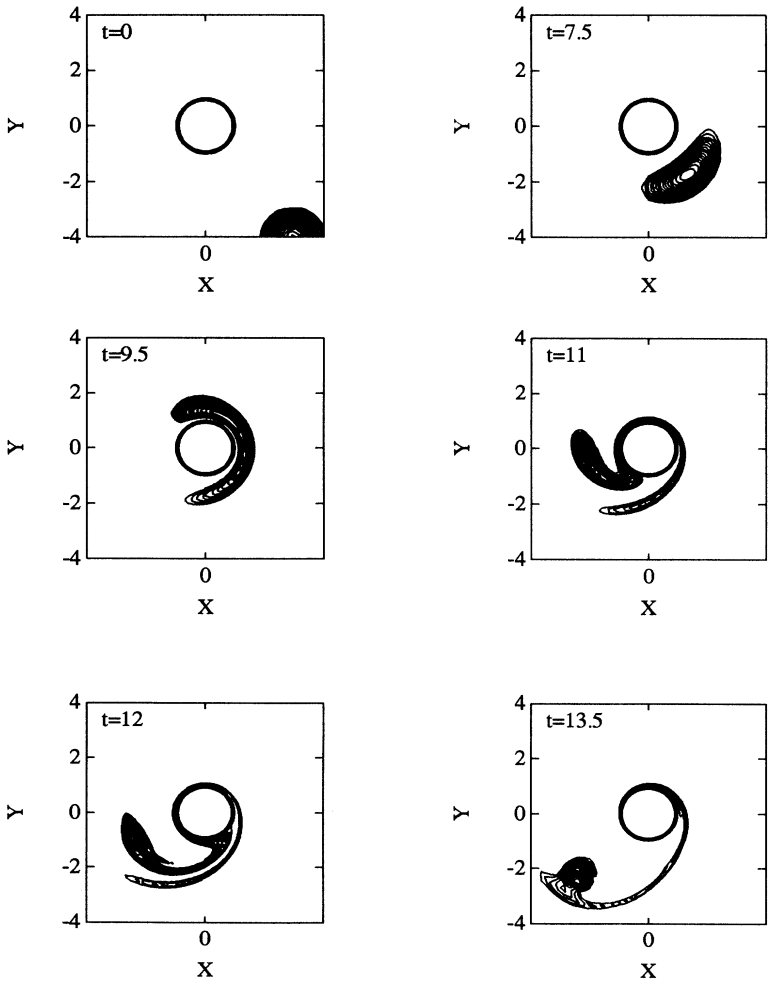

FIG. 6. Evolution of a Gaussian extended vortex of intensity $\sigma=-2.962962\ldots$, and size $S=0.75$ in a perturbed stream flow, in presence of a cylindrical body. Initial position of vortex center is $x_0=3, y_0=-4$. Vorticity contours (at levels from -6 to -1.8 by 0.2) are plotted for six different instants.

subsequent dynamics. This behavior is obviously significantly more complicated than can be observed in a point-vortex model, and implies possibilities for the classes of dynamical interactions that may occur in a real physical system. Currently, work is in progress to understand these more complicated systems and, in particular, the topological changes occurring in what originally was the point-vortex separatrices and hyperbolic points, and how to interpret their relevance to the extended system dynamics.

As discussed previously, dissipation in the extended system plays an important part in altering the dynamics of the vortex trajectories. In order to observe the global dissipation of the system, we show in Fig. 7 the time evolution of the enstrophy E, equal to the integral of the square of vorticity over the whole space,

$$E=\int\int \omega^2 dx\, dy\ , \quad -\infty \le x,y \le \infty\ , \tag{15}$$

normalized by its initial value, for the five simulations presented above. The two unperturbed evolutions (dashed lines) and the two capture evolutions (continuous lines) simply show a constant dissipation, with a roughly linear decay of enstrophy. This corresponds to the slow spreading of the vorticity distribution, with small changes due to different vortex distortions. For the chaotic capture events, however, we see significant decreases in the enstrophy as the vortex interacts with the body. This decrease is caused by stretching induced in the vortex as it passes over the cylinder, which in turn leads to a noticeable diffusion of vorticity allowing viscous effects to become much more significant. In the large-blob evolution (dotted line with circles) entropy decay is initially slower because of the smoother vorticity distribution (smaller initial absolute enstrophy), then for $10 < t < 15$ (during stretching and subsequent splitting of the blob in Fig. 6) the dissipation is locally intense, and dominates the vortex splitting-merging phenomena otherwise impossible in inviscid flow. Figures 4, 5, and 7 seem to therefore indicate that dissipation plays a relatively minor role in the dynamics of the simulation, except during a chaotic capture event. Even then, the primary effect of the dissipation may be to reduce the time period of a given capture event, but not to eliminate the existence of capture events *per se*. Such a conclusion would thus seem to strongly favor the idea that chaotic capture events should be observable in high Reynolds number real physical flows.

An important and striking characteristic of the chaotic capture events in the point vortex framework was the large pressure variations on the boundary of the body typically induced during a capture event [6]. In the present simulation we calculate instead the force acting on the body due to the vortex. This is an important quantity in applications to, e.g., wing surfaces, where aerodynamic loading can be critical. We note that the total force on the body includes the contributions due to the oscillatory perturbation, viscosity, etc., which have no relation to the vortex motion, so we consider only the dynamical action of the vortex. We calculate this effect via momentum-balance arguments [13,14] that in this case reduces to

$$\mathbf{F}=\frac{d\mathbf{I}}{dt}\ , \tag{16}$$

where $\mathbf{F}$ is the total force acting on the body, and $\mathbf{I}$ is the impulse given by

$$\mathbf{I}=\int\int \mathbf{u}\, dx\, dy\ , \quad -\infty \le x,y \le \infty\ ,$$

$$=\frac{1}{2}\int x \wedge \omega\, dx\, dy\ , \tag{17}$$

where $\wedge$ denotes exterior product and $\mathbf{u}$ denotes the velocity.

In Figs. 8 and 9 we show the time evolution of the longitudinal and transversal force acting on the body, F_x

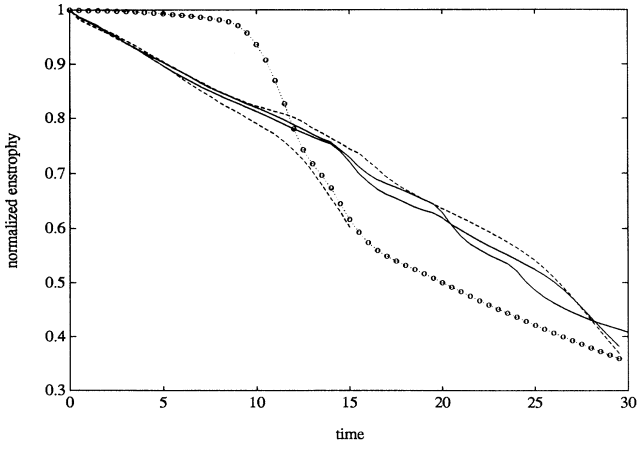

FIG. 7. Time evolution of the enstrophy (normalized by its value at $t=0$) for the five different evolutions of the extended vortices of the previous plots. Unperturbed evolutions (dashed lines), capture events (continuous lines), and large vortex (dotted line with circles).

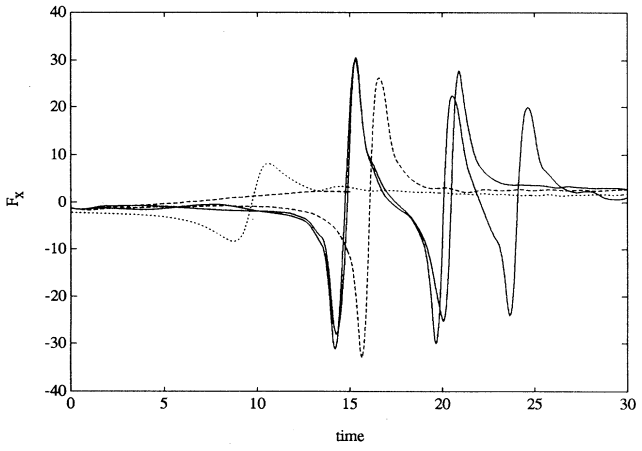

FIG. 8. Time evolution of the longitudinal force, for the five different evolutions of the extended vortices in the previous plots. Unperturbed evolutions (dashed lines), capture events (continuous lines), and large vortex (dotted line).

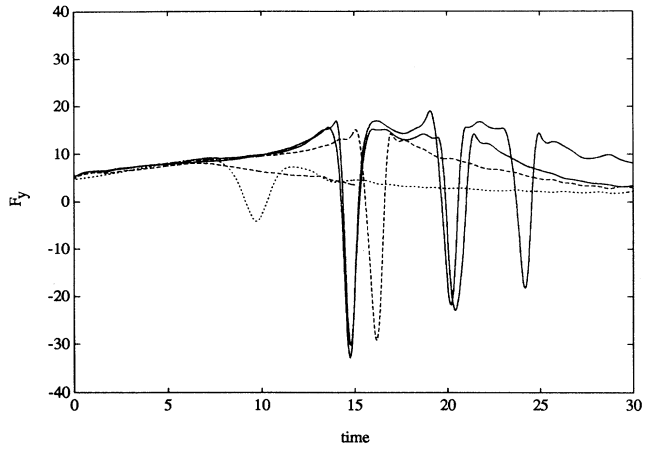

FIG. 9. Time evolution of the transversal force, for the five different evolutions of the extended vortices in the previous plots. Unperturbed evolutions (dashed lines), capture events (continuous lines), and large vortex (dotted line).

and F_y, respectively, for the unperturbed evolutions of Fig. 3 (dashed lines), the perturbed evolutions of Figs. 4 and 5 (continuous lines), and the large vortex evolution of Fig. 6 (dotted line). We can observe that the force is small until the vortex passes very close to the body surface, when the force on the wall abruptly increases. The body force then changes sign in a small time interval. Such a phenomenon occurs several times consecutively when the vortex is captured.

In Fig. 10 we show a polar plot in the F_x-F_y plane of the evolution of the force, for the four simulations with relatively concentrated vorticity. In this representation we can see explicitly the magnitude and the direction of the force acting on the body due to the vortex. All the trajectories start and end close to zero, as they would if the trajectories extend toward $\pm$ infinity [slight inaccuracies are due to numerical derivatives occurring in Eq. (16)]. In the first unperturbed evolution, the vortex passes below the body far enough away so that the resulting dynamical action is very small. In the second unperturbed run (see Fig. 3) the vortex passes close to the body surface and produces intense dynamical action. When the vortex is captured the dynamical action does not change much in magnitude, because the finiteness of the vortex prevents it from getting too close to the body. This is in contrast to what was observed in the point-vortex model, where the pressure on the surface could increase orders of magnitude when the vortex approached the body closely. On the other hand, during capture the vortex revolves around the whole body and the force can be maximal in any direction. It appears that the force reaches relative maxima 3 times each revolution, with the direction of application changing quite suddenly. This strong "buffeting" of the body is entirely due to the effect of the vortex. Such behavior may therefore have significant implications for the design of bodies which may be subject to interaction with turbulent or coherent vortical structures in open flows.

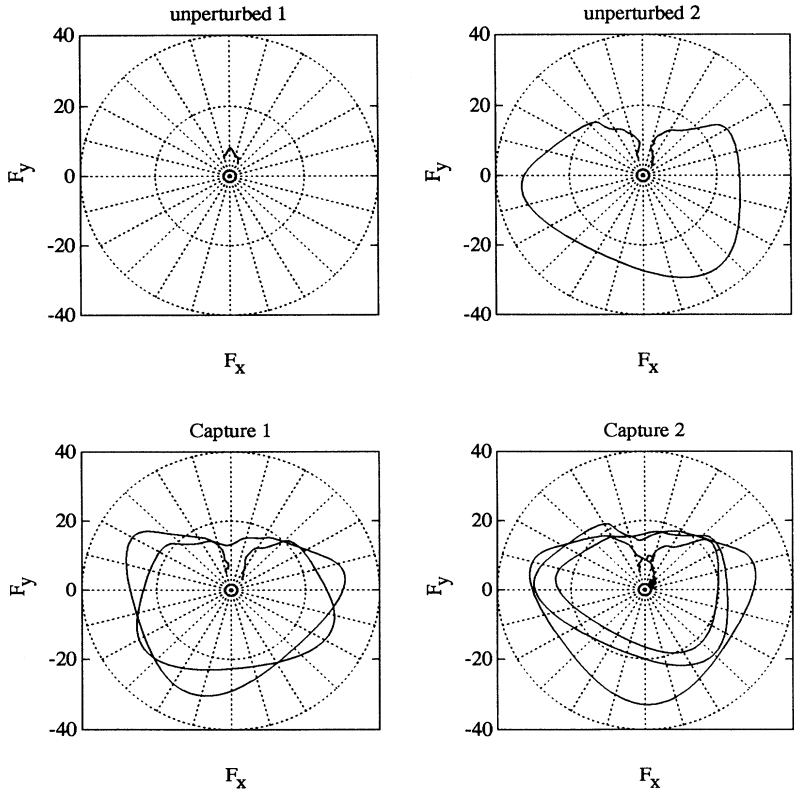

FIG. 10. Trajectories in the longitudinal, F_x, and transversal, F_y, force plane for the evolution of the force due to the vortices acting on the body. Unperturbed evolutions (above), and capture events (below) are shown.

V. CONCLUSIONS

The principal aim of the research described above was to investigate the possibility of the existence of chaotic trapping phenomena, as observed in point-vortex models, in systems with extended vorticity distributions. This was accomplished by developing a numerical scheme for the evolution of the extended vorticity distribution utilizing the Navier-Stokes equations. The simulations which were developed utilized a mixed spectral–finite-difference numerical algorithm. Free-slip boundary conditions were employed at the body surface in order to compare the results with previous Hamiltonian calculations.

The principal result of the work is that the chaotic capture phenomenon originally reported for the Hamiltonian point-vortex models exists also in the extended system, providing stronger evidence that the capture phenomenon may exist in real physical flows. Perhaps the most surprising of the above results is that much of the phase-space structure of the Hamiltonian formulation persists in extended systems, even for vortex distribution sizes which are relatively large when compared with the system length scales. For somewhat compact vorticity distributions, the dynamical behavior of the extended vortex along the original Hamiltonian separatrices and fixed points is very similar to the point-vortex dynamics, and even parameter ranges for high probability of capture are quite similar. Although it is difficult to interpret the structure of separatrices and fixed points in the extended system, it is clear that the point-vortex models capture much of the qualitative behavior of the extended system, and can be used to guide analysis of more complicated systems.

For larger vorticity distributions (roughly >0.5 of the body radius), the effect of the internal degrees of freedom of the extended distribution provides the primary difference in the dynamics. Here, the extra degrees of freedom seem sufficient to induce chaotic behavior even without the need for an explicit perturbation of the system. The implications of this result are that such capture events may be more general and ubiquitous than the original Hamiltonian problem indicates. Additionally, for large distributions new classes of dynamical interactions can occur, specifically the tearing apart of the vortex as it interacts with the body. Here, part of the vorticity distribution can be torn away from the vortex and lost downstream, while the remaining part remains captured for a longer time. The results of these simulations thus indicate that the dynamics of the extended system may be significantly richer than the original Hamiltonian system, and warranting further investigations.

In analogy with the pressure calculations for the point-vortex system, the global dynamical force acting on the body has been calculated by the impulse theorem. It has been observed that during capture events, the force can change sign very rapidly a number of times. In fact it could be seen that the force vector rotates around the body reaching its maximum about 3 times every vortex revolution at unpredictable directions. The results described above also indicate that there is a significant amount of work necessary to more fully understand the dynamical behavior of the extended system for this class of physical systems. For example, the primary effect of the viscosity in the extended formulation seems to be the shortening of the vortex-body interaction time, while it does not seem to affect the relative probability of experiencing a capture event. Also, a more realistic reformulation of the problem will be to eventually include no-slip boundary conditions around the body, and to investigate the effect this has on the dynamical behavior. In this case the vorticity shed from the wall can be expected to interact with the primary vortex leading to the possibility of an induced vortex pairing. It should also be determined whether, for some choice of the parameters, the trajectories of the pair and the subsequent evolution of the vorticity (primary, secondary, or tertiary) remaining close to the body can exhibit unexpected behavior.

A full classification of all of these possibilities may eventually lead to a more accurate modeling of important applications such as the aerodynamic properties of bodies in the presence of atmospheric vorticity. For example, for steadily moving bodies with circulation, the stagnation points on the body influence the structure of the boundary layer separation and hence the drag and lift characteristics. It is clear that the dynamics resulting from a vortex capture could significantly change these characteristics leading, for example, to a stalling phenomenon.

ACKNOWLEDGMENTS

The authors would like to thank Evgeny Novikov for enlightening discussions. The authors would also like to acknowledge the use of Cray Y-MP computer resources made possible by a grant from the San Diego Supercomputer Center at UCSD. J.B.K. acknowledges partial support by the NSF Small Grant for Exploratory Research No. CTS 93-12100.

[1] M. R. Dhanak, J. Fluid Mech. **110**, 129 (1981).
[2] S. Ersoy and J. D. A. Walker, J. Fluid Mech. **185**, 569 (1987).
[3] G. Pedrizzetti, J. Fluid Mech. **245**, 701 (1992).
[4] B. Eckhardt and H. Aref, Philos. Trans. R. Soc. London. Sect. A 326, 655 (1988).
[5] M. Ding, C. Grebogi, E. Ott, and J. A. Yorke, Phys. Rev. A **42**, 7025 (1990).
[6] J. B. Kadtke and E. A. Novikov, Chaos (to be published).
[7] J. B. Kadtke, H. Luithardt, and G. Pedrizzetti (unpublished).
[8] S. Wiggins, *Chaotic Transport in Dynamical Systems* (Springer-Verlag, Berlin, 1992), Chap. 4.
[9] J. B. Kadtke, H. Luithardt, E. A. Novikov, and G. Pedrizzetti (unpublished).
[10] P. J. Roache, *Computational Fluid Dynamics* (Hermosa, Albuquerque, 1972).
[11] C. A. J. Fletcher, *Computational Techniques for Fluid Dynamics* (Springer-Verlag, Berlin, 1988).
[12] P. Justesen, J. Fluid Mech. **222**, 157 (1991).
[13] G. K. Batchelor, *An Introduction to Fluid Mechanics* (Cambridge University Press, New York, 1967).
[14] P. G. Saffman, *Vortex Dynamics* (Cambridge University Press, New York, 1992).